Locality of Conical Intersections in Semiconductor Nanomaterials

Journal:	*Physical Chemistry Chemical Physics*
Manuscript ID	CP-PER-03-2019-001584.R1
Article Type:	Perspective
Date Submitted by the Author:	09-May-2019
Complete List of Authors:	Levine, Benjamin; Michigan State University, Chemistry Peng, Wei-Tao; Michigan State University, Chemistry Esch, Michael; Michigan State University, Chemistry

Locality of Conical Intersections in Semiconductor Nanomaterials

Benjamin G. Levine*, Wei-Tao Peng, Michael P. Esch
Department of Chemistry, Michigan State University, East Lansing, MI 48824

* to whom correspondence should be addressed: blevine@msu.edu

Abstract

A predictive theory connecting atomic structure to the rate of recombination would enable the rational design of semiconductor nanomaterials for optoelectronic applications. Recently our group has demonstrated that the theoretical study of conical intersections can serve this purpose. Here we review recent work in this area, focusing on the thesis that low-energy conical intersections in nanomaterials share a common feature: locality. We define a conical intersection as local if a) the intersecting states differ by the excitation of an electron between spatially local orbitals, and b) the intersection is accessed when the energies of these orbitals are tuned by local distortions of the geometry. After illustrating the locality of the conical intersection responsible for recombination at dangling bond defects in silicon, we demonstrate the locality of low-energy conical intersections in cases where locality may be a surprise. First, we demonstrate the locality of low-energy self-trapped conical intersections in a pristine silicon nanocrystal, which has no defects that one would expect to serve as the center of a local intersection. Second, we demonstrate that the lowest energy intersection in a silicon system with two neighboring dangling bond defects localizes to a single defect site. We discuss the profound implications of locality for predicting the rate of recombination and suggest that the locality of intersections could be exploited in the experimental study of recombination, where spectroscopic studies of molecular models of defects could provide new insights.

1. Introduction

It is often stated that semiconductor nanomaterials sit between the molecular and the bulk material limits. They exhibit some properties familiar from these two limits, and other unique (and often tunable) properties that scale between them. Consistent with this view is the fact that the optical and electronic properties of these materials are determined by a combination of delocalized and localized electronic states. For example, it is well known that the absorption and emission spectra of well-passivated semiconductor nanoparticles often arise from quantum-confined electronic excited states—those that are delocalized over the full volume of the particle.[1, 2] Thus, the absorption and emission energies can be tuned by varying the size and shape of the particle.

In contrast, in many cases nonradiative recombination (NRR) of electron and hole is attributed to electronic states that are localized to a particular defect site.[3, 4] Developing a microscopic mechanistic understanding of NRR is crucial to the rational design of materials for applications such as solar energy conversion, light emission, and sensing. However, development of such understanding remains challenging, due in large part to the heterogeneous nature of nanomaterials. Unlike well-defined molecules, an experimentally prepared sample of nanoparticles contains particles of varying size, structure, and defect composition, and particles prepared under different conditions or in different labs are unlikely to be exactly the same. Experimental control and characterization of the surfaces of nanomaterials is a developing field.[5-8] Given this uncertainty, theory and simulation have played an important role in connecting structure to function in these materials.[9-15] However, the same heterogeneities and uncertainties that make experimental study difficult also plague theoretical studies, and the large size of nanomaterials (relative to molecules) necessitate significant approximations in their simulation.

Though theoretical methods for predicting quantum confinement effects are well established and quite accurate, the simulation of NRR is a less mature and rapidly developing area.

Because NRR typically occurs via the relatively local, molecule-like excited states of defects, it is natural to use ideas and methods from molecular photochemistry to model and understand it. Over the last several years, our group has done exactly this, employing the characterization of conical intersections between potential energy surfaces (PESs) as a tool for understanding NRR. Conical intersections are points in geometry space where states of the same spin are degenerate.[16, 17] At these points, the nonadiabatic coupling between electronic states is singular, and it is quite large in the surrounding region of geometry space. When this region is accessed, the nonadiabatic coupling facilitates fast and efficient nonradiative transitions between electronic states. Conical intersections have been implicated in the photochemistry of a wide range of molecules, and it is now well established that such intersections are ubiquitous features of the PESs of polyatomic systems.[18-22]

Our group has demonstrated that conical intersections are often associated with specific defects on the surfaces of semiconductor nanoparticles. Analysis of these defect-induced conical intersections (DICIs) has shed light on several mysterious features of the emission of silicon nanocrystals (SiNCs), which show great promise for applications in light emission.[23] Namely, we have demonstrated that nonradiative pathways associated with DICIs can explain the unusual particle size–independent luminescence energies of oxidized SiNCs[24-27] and the complex relationship between surface structure and luminescence yield in SiNCs.[28]

A predictive understanding of recombination requires an assessment of the universal features of conical intersections. One feature that, to date, appears to be universal is *locality*. When we describe a conical intersection as a local feature of the material, we mean that it meets

two criteria: 1) The electronic transition associated with the intersection is characterized by the transfer of an electron between two spatially local orbitals, and 2) the intersection is brought about by local distortions of the geometry that tune the energies of these local orbitals. In this perspective, we will discuss recent progress towards a mechanistic understanding of NRR via conical intersections, paying particular attention to their locality. After briefly reviewing the computational methods available to describe conical intersections in nanomaterials, we will present an illustrative example of the locality of DICIs. Then we will address several questions: Are conical intersections present in pristine nanocrystals? If so, do they remain local? Do DICIs remain local in systems with multiple defects? We will argue that locality is a universal feature of low-energy conical intersections, in semiconductors as well as in molecules, and therefore that understanding the local electronic features of materials is essential to predicting a material's propensity for NRR. We will conclude by discussing important consequences of the locality of conical intersections for both the fundamental physics of NRR and for how they are studied both theoretically and experimentally.

2. Methods for Identifying Conical Intersections in Nanomaterials

Kohn-Sham density functional theory (DFT)[29] and its most common excited state extension, linear response time dependent (LR-TD-) DFT,[30, 31] have been established as methods of choice for modeling the electronic structures of nanomaterials in most contexts. This is because density functionals offer an excellent balance between the accuracy of the treatment of dynamical electron correlation and computational cost. However, DFT and LR-TDDFT are known to predict intersections between the electronic ground and excited states with incorrect dimensionality.[32] Conical intersections exist not as single points, but as $3N$-2 dimensional seams in geometry space, where N is the total number of atoms. DFT/LR-TDDFT, however, predicts intersection seams that

are incorrectly 3*N*-1 dimensional.[32] Thus, in their most widely used forms these otherwise useful methods cannot be applied to model conical intersections. Several DFT-like methods that can compute conical intersections with proper dimensionality have been proposed, based either on modifications of the LR-TDDFT response formalism[33-39] or incorporation of a DFT-like description of electron correlation into a multireference framework.[40-43] These methods have yet to be widely adopted, though they show great promise.

In molecular photochemistry, the most widely used electronic structure method for studying conical intersections is the state-averaged complete active space self-consistent field (SA-CASSCF) method.[44] Until recently, however, its large computational cost prevented the application of SA-CASSCF to larger nanoscale systems. Advances in electronic structure theory and high-performance computing have enabled the study of conical intersections in nanoscale systems for the first time. These advances, which have recently been reviewed in detail,[45] are briefly summarized here.

The large computational cost of multireference electronic structure methods such as SA-CASSCF has been overcome by enlisting graphics processing unit (GPU) accelerators.[46, 47] GPUs are massively parallel computer processors—with thousands of floating point processors on a single chip—designed for graphical applications such as computer games. Their excellent floating point performance and high memory bandwidth make them ideal for floating point–intensive tasks like electronic structure calculations. With careful implementation, two-order-of-magnitude speed-ups have been obtained,[46, 48, 49] enabling the application of multireference methods to nanoscale systems.

However, SA-CASSCF suffers two additional problems that limit its applicability to nanoscale systems: 1) excitation energies computed at the SA-CASSCF level of theory are not size

intensive (that is, the error in computed excitation energies increases with the increase in the system size),[50] and 2) the higher densities of single-electron states (orbitals) in large systems can lead to instabilities in the SA-CASSCF equations, in turn resulting in discontinuous PESs and convergence difficulties.[51-53] Both of these problems can be attributed to the fact that the orbital coefficients and configuration interaction (CI) expansion vectors are optimized simultaneously in SA-CASSCF. These problems can be overcome by replacing SA-CASSCF with complete active space configuration interaction (CASCI) methods. In a CASCI calculation, the orbital and CI vector optimizations are separated into two steps. Many variations on CASCI exist, differing in the recipe used to determine the orbitals.[50, 54-59] Because the orbital coefficients and CI vector are not simultaneously optimized, CASCI is variationally inferior to SA-CASSCF. However, because issues with size intensivity and numerical instability can be avoided, CASCI methods can be designed to be qualitatively superior to SA-CASSCF in these specific ways. CASCI methods are also often computationally cheaper than SA-CASSCF, though the computational scaling is the same, so this is a more minor advantage. For studying conical intersections in nanomaterials, preferred methods include the configuration interaction singles natural orbital (CISNO)[50] and floating occupation molecular orbital (FOMO) approaches.[57, 58] CISNO and FOMO both exhibit numerical stability and size intensive excitation energies.[50] Fast GPU-accelerated implementations of both exist in the TeraChem software package.[46, 48, 49, 60]

Analytic calculations of gradients and nonadiabatic coupling vectors[61, 62] enable the fast optimization of conical intersections and ab initio molecular dynamics (AIMD) simulations in nanoscale systems. Numerous methods exist for conical intersection optimization.[63-68] These methods identify minimal energy conical intersections (MECIs), points of locally minimal energy on the seam of degeneracy. MECIs can be thought of in analogy to transition states in ground state

chemistry; they are representative of the region of geometry space in which transitions between electronic states are highly efficient, just as transition states are representative of the region of geometry space in which the molecule is likely to transition between reactant and product.

CASCI is a useful zeroth order method, but calibration to methods that accurately describe dynamic correlation is essential to achieving accurate results. Standard multireference wave function–based methods including dynamic correlation are not presently applicable to nanoscale systems due to their high computational cost. However, as will be discussed below, cluster models of defects provide excellent molecule-sized (ca. 10-20 heavy atoms) models for the study of NRR. Application of accurate dynamically correlated methods such as multi-state complete active space second order perturbation theory (MS-CASPT2)[69, 70] and multireference configuration interaction (MRCI) to systems of this size is routine, enabling the careful quantification of errors arising from the absence of dynamic electron correlation in the CASCI treatment of larger nanoscale systems.

One key advantage of the conical intersection theory of NRR relative to the more widely applied band theory is worth mentioning in this context. Band theory assumes interactions between charge carriers are negligible. This may be an excellent approximation for delocalized electronic states in crystalline materials but likely breaks down when charge carriers localize to defects. In contrast, PESs can, in principle, be computed exactly, including arbitrarily strong correlation between charge carriers. As such, the conical intersection approach to modeling recombination inherently includes fewer approximations than band theory.

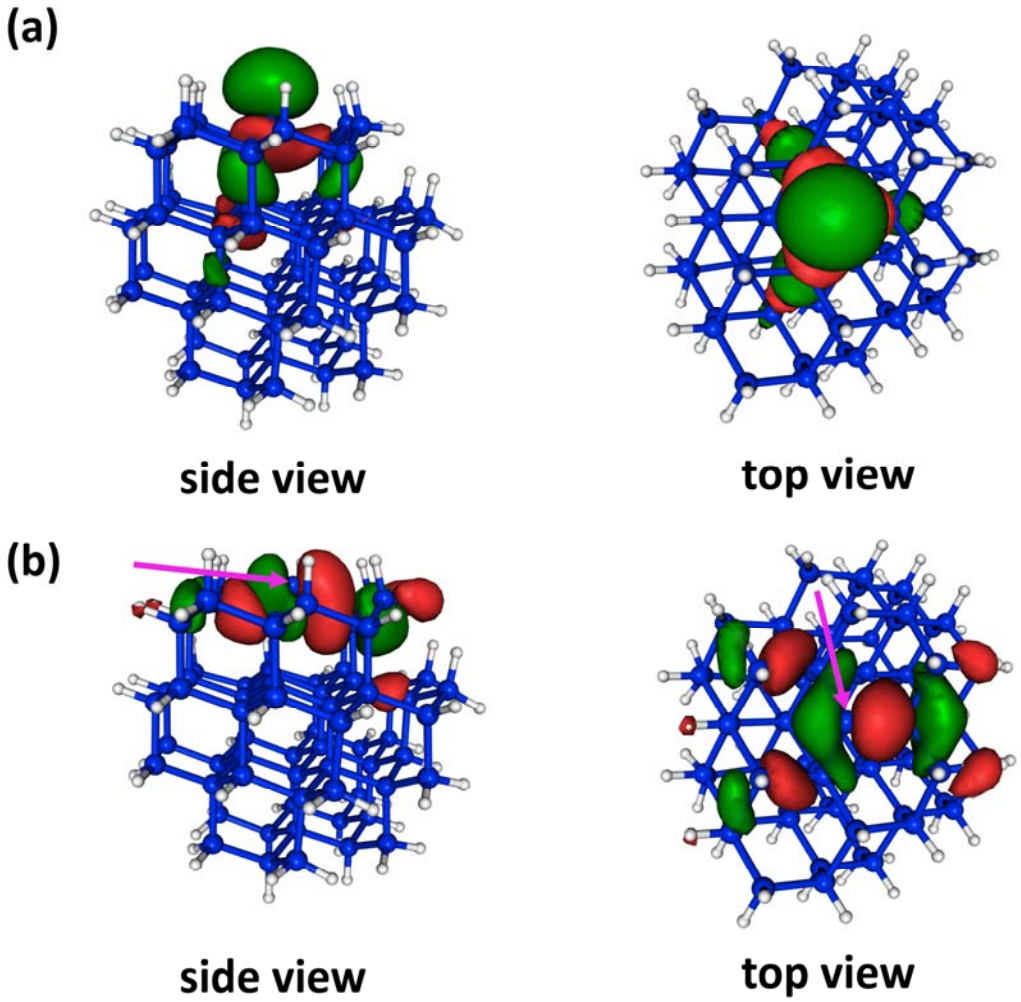

Figure 1. The MECI between the ground and first excited state of the dangling bond–containing $Si_{72}H_{63}$ SiNC. Panel a) shows the n orbital and panel b) shows the σ orbital. In panel b) the defect site is marked by a purple arrow.

3. Locality of the Dangling Bond DICI

Here we will analyze one of the most well-known nonradiative centers, the silicon dangling bond defect, as an illustrative example of the locality of DICIs. It is well established that dangling bond defects—three-coordinate silicon atoms—introduce efficient pathways for NRR.[71-74] In the neutral state of the defect, a single electron populates a nonbonding (n) hybrid orbital. Passivation

of this defect by hydrogenation and hydrosilylation are well known approaches to eliminate these centers.[75, 76] The textbook mechanism of NRR at these defects is as follows:[10, 73] 1) A charge carrier (either electron or hole) can become trapped in the n orbital. 2) A second charge carrier of opposite charge (either a hole in the valence band or electron in the conduction band) then recombines with the trapped carrier. In this mechanism the trapped charge carrier is stabilized by a local distortion of the coordination environment of the under-coordinated silicon atom; in the case of a trapped electron (hole) the under-coordinated atom pyramidalizes towards a more sp^3-like structure (flattens towards a more sp^2-like structure). Prior to recombination, the second carrier occupies either the valence or conduction band and is therefore delocalized.

Using AIMD simulations based on FOMO-CASCI, we have recently revisited the mechanism of NRR in these materials.[26] This work demonstrated that this process can be described in terms of conical intersections and that going beyond the independent particle (band) picture yields deeper insights into the dynamics of NRR. The structure of the MECI between the ground and first excited electronic states of a dangling bond–containing SiNC ($Si_{72}H_{63}$; 1.7 nm diameter) is shown in Figure 1. In this model, all surface sites aside from the dangling bond defect are passivated by hydrogen atoms. The two orbitals involved in the electronic transition at the conical intersection are also pictured. The orbital pictured in Figure 1a is precisely the n orbital described above. This orbital is singly occupied in the electronic ground state, and takes on a second electron in the lowest excited state. The second orbital involved in the intersection, which is doubly occupied in the ground electronic state and singly occupied in the first excited state, is pictured in Figure 1b. Contradicting conventional wisdom, this orbital is not delocalized over the entire particle. Instead, the electron density of this Si-Si σ bonding orbital is local to the few atoms surrounding the defect sight. This localization is attributed in part to the Coulomb attraction of

the hole populating this orbital for the electrons occupying the n orbital. This attraction is neglected in standard band theory.

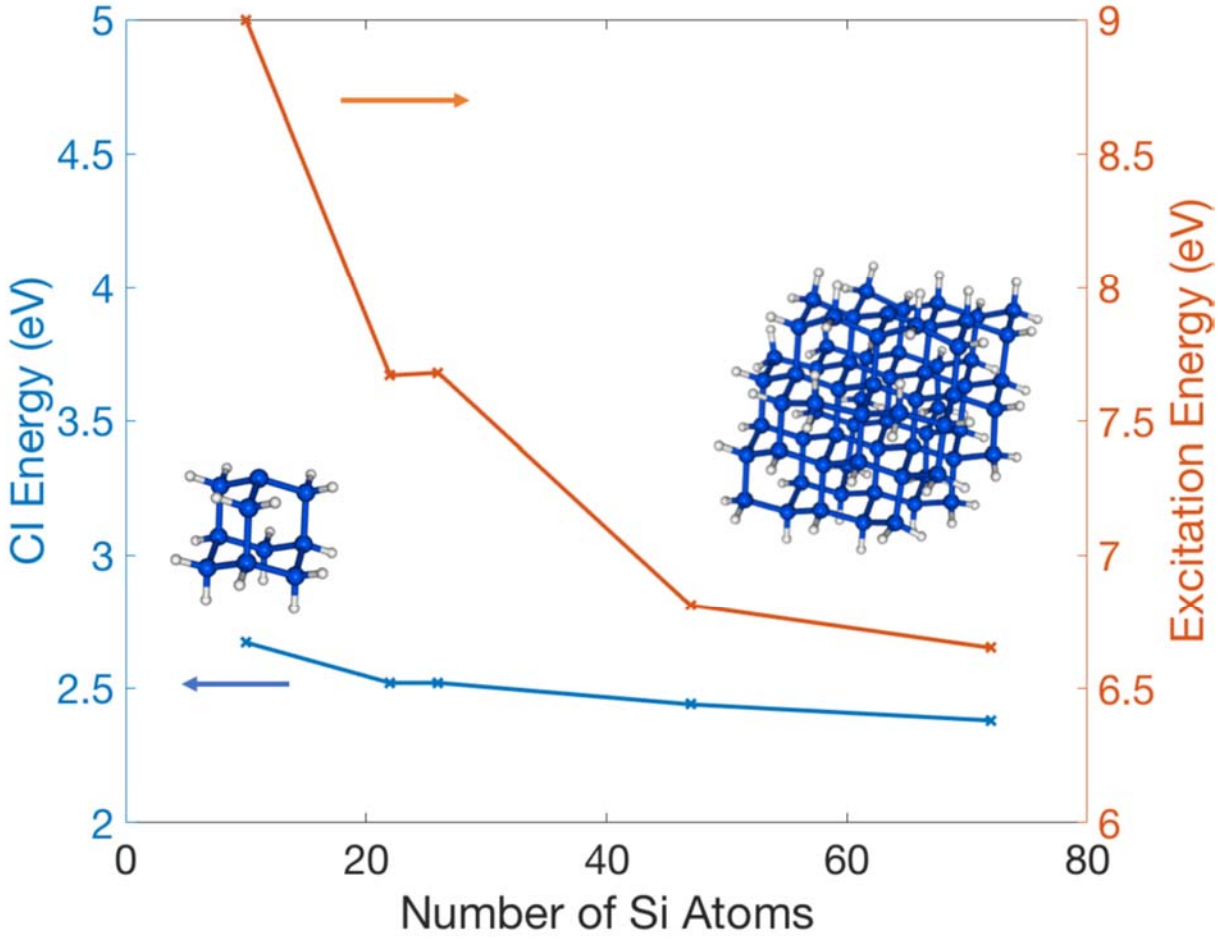

Figure 2. The energies of the MECIs in dangling bond–containing particles ranging from $Si_{10}H_{15}$ to $Si_{72}H_{63}$. Left and right insets show the smallest and largest clusters, respectively.

At the intersection, the ground and first excited states are degenerate. This degeneracy is brought about by local geometric distortions that tune the energies of these two orbitals. Two specific distortions are observed: a pyramidalization motion that tunes the energy of the n orbital (just as described above) and an asymmetric stretching motion of the three Si-Si bonds surrounding the defect Si atom, which stabilizes the hole in the σ bonding orbital. This second motion is the

direct consequence of the localization of this σ bonding orbital and drives further localization because the hole is further stabilized by stretching. This motion is not predicted by the standard band model of this process and could potentially serve as an experimental signature for recombination by dangling bond.

A very important consequence of the locality of these intersections is that the energies of these intersections relative to the ground state minimum energy is relatively insensitive to the size of the particle. Figure 2 shows the energies of structurally similar MECIs in particles ranging in size from $Si_{10}H_{15}$ (a molecular model based on sila-adamantane) to the $Si_{72}H_{63}$ SiNC described above. The vertical excitation energies of the quantum confined excitons in pristine SiNCs of the same sizes are shown for comparison. The changes in the MECI energies are slight compared to those in the vertical excitation energies of the quantum confined states. Specifically, the MECI energy decreases by 0.29 eV (from 2.67 to 2.38 eV) while the vertical excitation energy decreases by over 2 eV. Similar size-insensitivity has been predicted for the energies of DICIs associated with silicon epoxide and Si=O double bond defects.[25] The consequences of the size-insensitivity of the MECI energies are discussed in Section 6, but first we will consider whether locality is a feature specific to DICIs or a general feature of conical intersections in all systems.

4. Do Conical Intersections in Pristine Nanocrystals Remain Local?

We have established that the conical intersections associated with dangling bond defects are local; they arise due to local distortions of the nuclear structure around the defect which tune the energy of a local electronic transition. This raises interesting questions. Do pristine nanoparticles—the lowest excitations of which are typically delocalized—exhibit conical intersections? If so, are these intersections local like DICIs are, or do they involve nonlocal distortions of the nuclear structure and/or nonlocal electronic transitions? Note that conical

intersections in pristine materials are just as important as DICIs. It is these intersections that correspond to the inherent recombination mechanism of the material, controlling its photoluminescence yield in the absence of specific defects.

To address the questions above we will consider a pristine hydrogen-terminated SiNC, $Si_{72}H_{64}$. We have identified a MECI in this nanoparticle at the FOMO-CASCI/LANL2DZ[77] level of theory and present it in Figure 3. A two-electron/two-orbital active space was chosen. The structure is shown in Figure 3a, with three silicon atoms labeled Si1, Si2, and Si3. In the ground state structure (not shown) covalent bonds connect Si1 with Si2 and Si1 with Si3. At the MECI structure, however, these bonds are significantly stretched. Specifically, the bond lengths increase to 3.08 and 3.19 Å at the MECI from 2.36 Å at the ground state minimum structure. At least in this case, it appears that the nuclear distortions associated with a conical intersection in a pristine nanoparticle are local, despite the absence of a local defect.

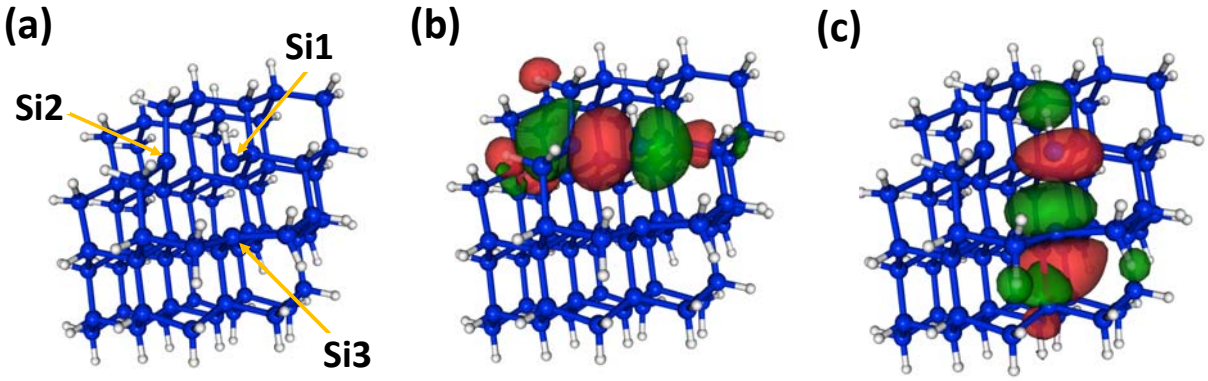

Figure 3. The structure of the MECI of the pristine $Si_{72}H_{64}$ SiNC is shown in panel a. The PONOs, σ and σ*, are presented in panels b and c, respectively.

The partially occupied natural orbitals (PONOs) associated with the intersecting electronic states are pictured in Figures 3b and 3c. (The PONOs are computed as the eigenvectors of the state-averaged one-electron reduced density matrix, averaged over the two intersecting states.) It can be seen that these orbitals are local to the region of nuclear distortion. One orbital is the σ bonding orbital between Si1 and Si2 (state-averaged occupation number 1.5), while the other is the σ antibonding orbital between Si1 and Si3 (σ*; state-averaged occupation number 0.5). The intersection occurs between a state in which σ is doubly occupied and one in which σ and σ* are each singly occupied. One can think of this transition as the creation of a self-trapped exciton.

Having established the locality of the MECI in a pristine hydrogen-terminated SiNC, we now ask whether this self-trapping mechanism is general. We will argue that this mechanism is likely general and that energetically accessible intersections involving delocalized excitations and geometric distortions are unlikely under any circumstances. Our argument is based on the deep understanding of conical intersections that has been developed in the field of organic photochemistry over many years. The self-trapped intersection in a pristine SiNC is an example of a biradicaloid intersection. Biradicaloid intersections arise when nuclear distortions bring about near degeneracy of the highest occupied and lowest unoccupied molecular orbitals (HOMO and LUMO). At such geometries the configuration in which the HOMO is doubly occupied and that in which the HOMO and LUMO are each singly occupied may become degenerate, resulting in a conical intersection. A detailed explanation of biradicaloid intersections can be found in the classic text on organic photochemistry by Michl and Bonacic-Koutecky.[78]

Our argument that energetically accessible conical intersections will, in general, involve only local distortions of the electronic structure and geometry arises from this biradicaloid picture. Imagine a large system, such as a nanoparticle, in which the HOMO and LUMO are delocalized

over the entire system. One could, in principle, bring the energies of these orbitals into near degeneracy by distorting the geometry of the entire system (e.g. symmetrically stretching all bonds in the system to bring a bonding HOMO and antibonding LUMO into degeneracy.) It is very likely that a conical intersection could be achieved in this way, but the energetic cost would be enormous. The energy of every electron pair involved in chemical bonding would be increased, resulting in a conical intersection geometry with a very high energy.

Local nuclear distortions, on the other hand, break the effective symmetry of the system, resulting in a localization of the HOMO and LUMO. For example, stretching one or two chemical bonds will significantly increase the energies of one or two pairs of electrons, but leave the remaining electrons near their ground states energies. In this way the localized HOMO and LUMO are tuned to near degeneracy, yielding a relatively low-energy conical intersection.

This effect can be clearly illustrated using a classic example of a series of organic molecules with conical intersections: short polyenes.[79, 80] MECI geometries of the four shortest polyenes with HOMOs and LUMOs (computed as state-averaged PONOs) are presented in Figure 4a. (See Supplementary Information for computational details.) In all four cases, the intersection is reached by twisting of a terminal carbon-carbon double bond and pyramidalization ($sp^2 \rightarrow sp^3$ hybridization) of the terminal CH_2 group. Together, these distortions bring about near degeneracy of the HOMO and LUMO, which manifests in a conical intersection. Note that both orbitals are local to the region of the twisted bond, in contrast to the lowest excitation at the ground state minimum energy structure, which is well known to be delocalized over the entire π system (not shown). This is a prime example of our argument; local distortions of the geometry localize the HOMO and LUMO and bring them into near degeneracy, leaving the remaining electrons relatively unperturbed.

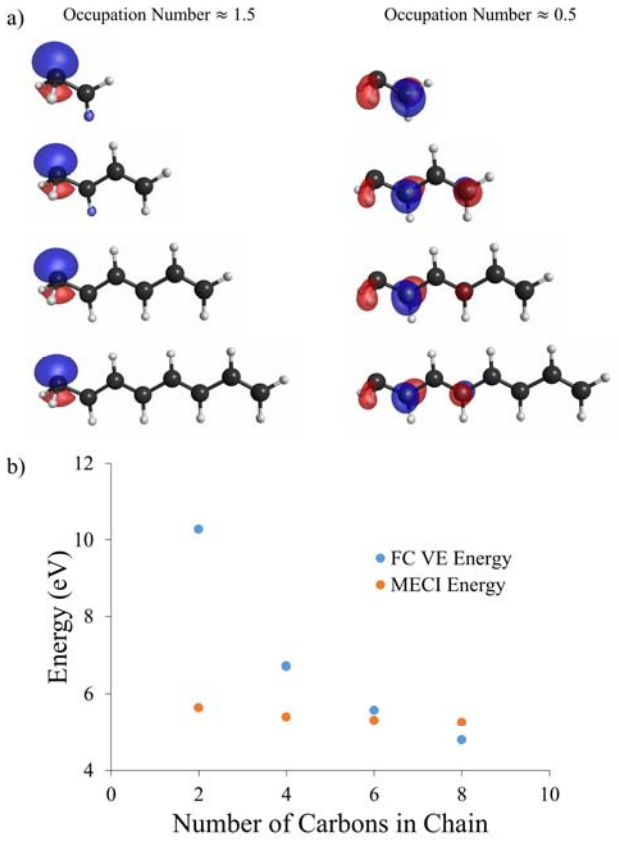

Figure 4. a) The HOMO (state-averaged occupation number ~1.5; left) and LUMO (state-averaged occupation number ~0.5; right) from biradicaloid intersections in a series of linear polyenes. b) The vertical excitation (VE) energy at the Franck-Condon (FC) point (blue) and the energy of the MECI (orange) relative to the ground state minimum energy are presented as a function of carbon chain length.

The locality of the intersections can also be seen in their energies. Figure 4b shows two energies as a function of the number of carbons in the polyene chain: the energy of the lowest singlet excited state at the ground state minimum energy structure (vertical excitation energy) and the energy of the MECI. Both energies are computed relative to the ground state minimum energy.

Notice that the vertical excitation energy, which corresponds to a delocalized excited state, decreases sharply with increasing chain length, consistent with quantum confinement effects. However, the MECI energy stays nearly constant. The weak dependence of the MECI energy on system size is a quantitative marker of the locality of a conical intersection.

The consequences of this size insensitivity are also well illustrated by this series of short polyenes. Upon vertical excitation, both ethylene and s-trans-1,3-butadiene have more than enough energy to reach their associated intersections, and thus efficiently decay nonradiatively to the ground state. Vertically excited all-trans-1,3,5,7-octatetraene, on the other hand, lacks the energy to reach the intersection in Figure 4, consistent with the knowledge that it fluoresces.[81] It must be noted that, though illustrative, this presentation of the photochemistry of polyenes is dramatically oversimplified. The PESs of polyenes are complicated by the presence of many conical intersections not presented in Figure 4.[79, 80]

To date, all conical intersections that we have identified in nanomaterials are biradicaloid in nature,[24, 25, 27, 28, 82-85] with the single exception of the dangling bond described above. The dangling bond is simply a radical, but a similar energetic balance results in a conical intersection; the n and σ orbitals must be tuned to near degeneracy to bring about a conical intersection between PESs. Other examples of conical intersections in molecules include tetraradicaloids,[86] which again arise when local geometric distortions tune the energies of local orbitals into near degeneracy. In all of these cases, delocalized geometric distortions should be expected to result in a larger increase in the total energy than more localized distortions. Thus, the argument above can easily be generalized from biradicaloids to other common classes of conical intersections.

5. Does the Presence of Multiple Defects Affect the Locality of DICIs?

Our past studies of DICIs have focused on idealized nanoparticles containing a single defect, but a realistic nanoparticle may have more than one defect on its surface. A natural question is whether the defects behave independently of one another or interact, modifying the recombination mechanism. In other words, are DICIs local to a single defect even in the presence of multiple defects? With this question in mind we have studied pathways for nonradiative decay in nanoscale slab models of the silicon surface ($Si_{70}H_{68}$) containing pairs of dangling bond defects. The distance between dangling bond defects was varied from 3.9 to 10.3 Å, and the structure and energies of the intersection were analyzed. A publication describing a detailed study of this system, including dynamical simulations investigating the possibility of energy transfer between defects, is forthcoming. However, in this work we analyze an MECI to specifically address the question of whether non-radiative recombination pathways are affected by the presence of multiple defects in close proximity. The ground state of this system is a spin triplet, thus the intersection between the ground and first excited triple states is reported. It was computed at the FOMO-CASCI level with a 10-electron/6-orbital active space and the LANL2DZ basis set (five active electrons in three active orbitals on each defect).

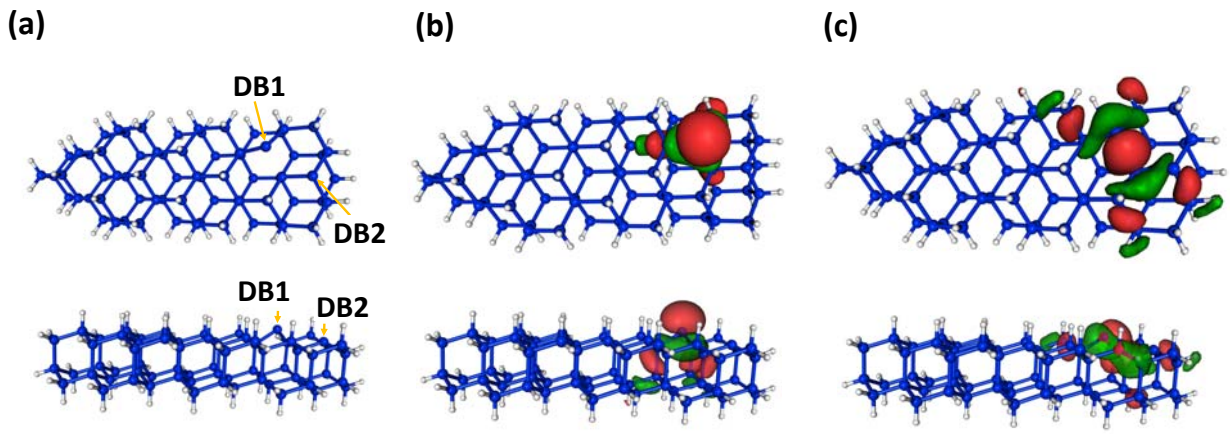

Figure 5. The MECI structure of a nanoscale slab with two dangling bond defects located at DB1 and DB2. The structure is shown in panel a, and the n and σ PONOs (state-averaged occupation number ~1.5 in both cases) are shown in panels b and c, respectively. The upper and lower pictures in each panel show the top and side views of the same geometry and orbital.

The MECI structure and state-averaged PONOs of a slab in which two dangling bond defects are separated by 3.9 Å (two Si-Si bonds) are presented in Figure 5. Just as in the case of the solitary dangling bond described above, the two PONOs are the n orbital of an under-coordinated silicon atom (DB1, in this case), and the σ bonding orbital on an adjacent Si-Si bond. The n PONO is not observed to delocalize to the other dangling bond. The σ orbital is somewhat more delocalized by nature, even in the case of a solitary dangling bond (Figure 1b). However, even in this case the σ orbital remains centered on the most stretched Si-Si bond adjacent to DB1.

The geometric distortions associated with this intersection are also localized to the DB1 site. The side view (Figure 5a bottom) shows the DB1 site to be noticeably more pyramidalized (sp^3-like) than DB2. This hybridization stabilizes the localization of a second electron in the n orbital in one of the intersecting states. The longest of the three Si-Si bonds surrounding DB1 is

3.00 Å, compared to values of 2.36, 2.39, and 2.41 Å surrounding DB2. It is this longest bond upon which the σ orbital has the most density (Figure 5c). A similar MECI has been identified with the excitation localized on DB2, rather than DB1 (not shown).

Just as the electronic excitation and associated geometric distortions are local to the defect site, energetics also suggest the locality of the intersection. The MECI of the two-dangling-bond slab pictured in Figure 5 is 2.33 eV above the ground state minimum energy, compared to 2.38 eV for the isolated dangling bond defect described above, suggesting only a very week interaction between defects. Comparison to a second slab system in which DB1 and DB2 are separated by 10.3 Å rather than 3.9 Å (6 Si-Si bonds rather than 2 Si-Si bonds) also suggests a very weak interaction; the MECI in the 10.3 Å system (not pictured) is 2.41 eV above the ground state minimum energy—less than 0.1 eV above that of the 3.9 Å system.

Thus, intersections in systems with multiple defects appear to very closely resemble those in systems with one isolated defect. In light of the arguments made in Section 4 regarding the locality of intersections in pristine systems, this is not at all surprising. One could likely bring about a nonlocal conical intersection by distorting the geometry around both defects symmetrically. However, this will disturb many electrons, resulting in a high energy. Distorting the structure of a single defect disturbs fewer electrons and can therefore bring about a conical intersection at a lower energy.

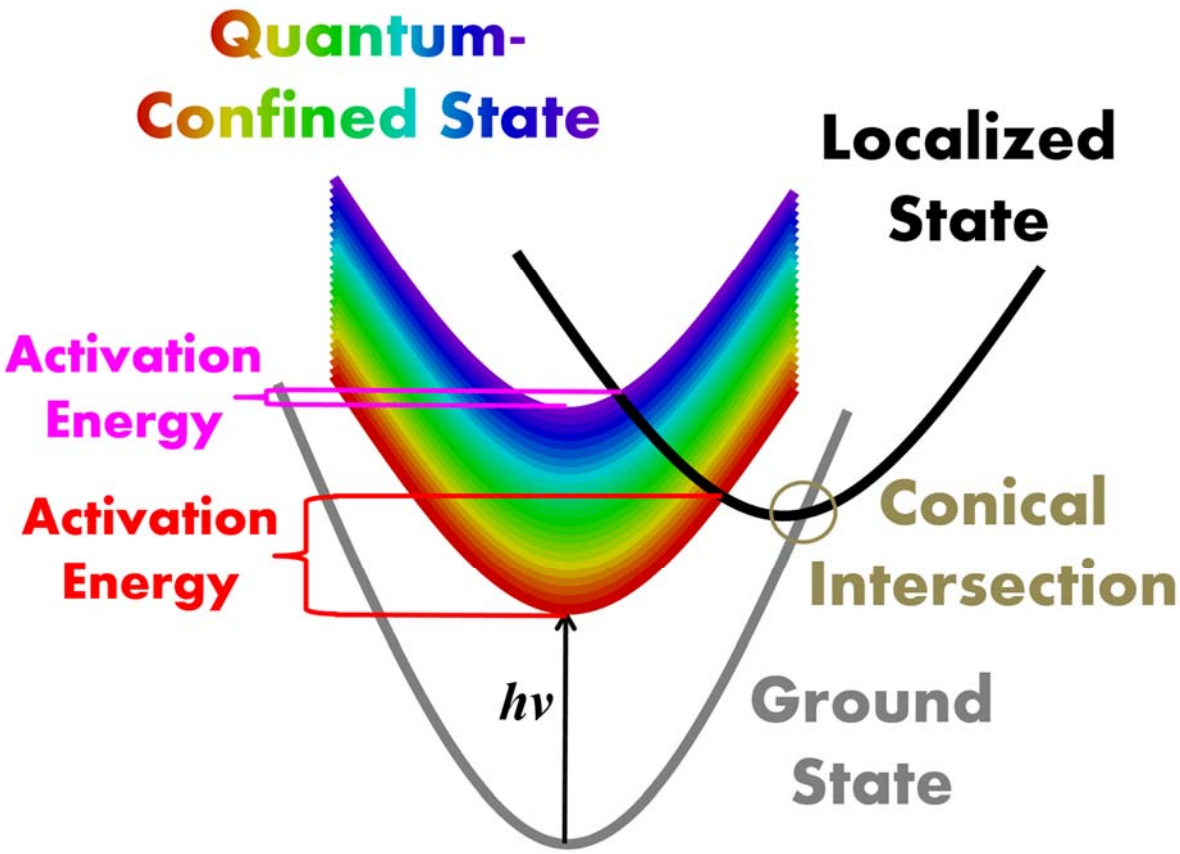

Figure 6. Illustration of the effect of particle size on the activation energy for localization. The PES of the localized state (whether defect-localized or self-trapped) is shown in black. The energy of this state is assumed to be particle size independent. A band of parallel PESs for quantum-confined states corresponding to different particle sizes is shown in rainbow colors. Colors ranging from red to purple correspond to nanoparticles ranging from larger to smaller. The localization process is the rate-limiting step in recombination, assuming fast subsequent passage through the conical intersection between the localized and ground electronic states. The activation energies are shown for the extreme red and purple cases to illustrate the strong dependence of the activation energy on particle size.

6. Conclusions

In this perspective we have argued that, in general, low energy conical intersections will involve local electronic transitions and local distortions of the geometry, even in nanoscale systems whose vertical excitations are strongly delocalized. We note, however, that our arguments are general to all areas of photochemistry and photophysics. Whether studying molecules, semiconductor nanocrystals, or larger bulk systems, our argument holds. The energies of localized electronic transitions can be tuned by local geometric distortions, and local geometric distortions result in a smaller increase in the total energy of the system than global distortions.

The locality of conical intersections has important consequences for the study of NRR in nanomaterials. The first of these consequences arises from the fact that the energies of local conical intersections are relatively insensitive to system size. Unintuitively, such size-insensitive intersection energies lead to strongly size-sensitive rates of non-radiative recombination. We have argued this point in detail in several other publications,[25-27, 45] and briefly recap here. The luminescence of SiNCs arises from a quantum-confined (delocalized) exciton.[87] NRR of this exciton in a semiconductor nanocrystal via conical intersection is (at least) a two-step process, as illustrated in Figure 6. The first step is localization of the excitation to the site of the conical intersection. This site is often a defect on the surface, but localization can also occur via self-trapping as in the pristine SiNC described in Section 4. This localization is followed by relaxation to the electronic ground state through the conical intersection (whether defect-induced or self-trapped). This latter process is often fast and efficient, though the rate will depend on the PES topography, as has been discussed in detail in the context of small molecules and theoretical models.[88, 89] The localization process, on the other hand, may be an activated process and is likely to be rate limiting. At its simplest, the localization process can be thought of as Marcus-like;[90, 91]

the barrier to localization is the crossing between a quantum-confined electronic state and the localized state associated with the conical intersection. We have argued that the energy of the localized state (black curve in Figure 6) is size-independent, but the energy of the quantum-confined state (parallel rainbow-colored states in Figure 6) is well-known to depend strongly on the size of the nanoparticle. Thus, the activation energy, and therefore the rate of localization, will depend strongly on particle size (illustrated for the extreme red and purple cases in Figure 6). We have previously predicted the size dependence of these activation energies for recombination at dangling bond[45] and oxygen-containing[25] defects on the silicon surface, finding that this size-dependent rate can explain the experimentally observed size-independent ensemble luminescence energy of oxidized SiNCs.[92]

The second important consequence of the locality of conical intersections in semiconductor nanomaterials is that it emboldens us to study molecule-sized cluster models of defects. The advantage of employing small cluster models is that we can apply more sophisticated theoretical techniques that are typically limited to small molecules, e.g. nonadiabatic AIMD simulations based on a multireference description of the electronic structure and dynamically correlated wave function theories, such as MS-CASPT2 and MRCI.

Looking to the future, the locality of conical intersections also encourages the experimental study of molecular models of defects. Traditional and ultrafast spectroscopic studies of molecular models of semiconductors would provide an unprecedentedly detailed look at defect photophysics. Not only would such studies provide insights into the photophysics of specific defects, but they would also provide experimental signatures that could be used to identify and study defects in heterogeneous samples of larger nanoparticles.

Conflicts of Interest

There are no conflicts to declare.

Acknowledgements

We gratefully acknowledge financial support from the National Science Foundation under grant CHE-1565634 and Michigan State University through a Strategic Partnership Grant. We are also grateful for a generous allocation of supercomputer time from the Extreme Science and Engineering Discovery Environment (XSEDE), which is supported by the NSF under Grant ACI-1548562 (allocation CHE-140101).

References

1. L. E. Brus, *J. Chem. Phys.*, 1984, **80**, 4403-4409.
2. A. I. Ekimov, A. L. Efros and A. A. Onushchenko, *Solid State Commun.*, 1985, **56**, 921-924.
3. W. Shockley and W. T. Read, *Phys. Rev.*, 1952, **87**, 835-842.
4. R. N. Hall, *Phys. Rev.*, 1952, **87**, 387-387.
5. Z. Hens and J. C. Martins, *Chem. Mater.*, 2013, **25**, 1211-1221.
6. A. J. Morris-Cohen, M. Malicki, M. D. Peterson, J. W. J. Slavin and E. A. Weiss, *Chem. Mater.*, 2013, **25**, 1155-1165.
7. J. Owen, *Science*, 2015, **347**, 615-616.
8. M. A. Boles, D. Ling, T. Hyeon and D. V. Talapin, *Nat. Mater.*, 2016, **15**, 141-153.
9. A. L. Efros, M. Rosen, M. Kuno, M. Nirmal, D. J. Norris and M. Bawendi, *Phys. Rev. B*, 1996, **54**, 4843-4856.
10. C. Delerue and M. Lannoo, *Nanostructure: Theory and Modelling*, Springer-Verlag, Berlin, 2004.
11. J. R. Chelikowsky, M. M. G. Alemany, T. L. Chan and G. M. Dalpian, *Rep. Prog. Phys.*, 2011, **74**, 29.
12. L. J. Wang, R. Long and O. V. Prezhdo, in *Annual Review of Physical Chemistry, Vol 66*, eds. M. A. Johnson and T. J. Martinez, Annual Reviews, Palo Alto, 2015, vol. 66, pp. 549-+.
13. A. Fernando, K. L. Dimuthu, M. Weerawardene, N. V. Karimova and C. M. Aikens, *Chem. Rev.*, 2015, **115**, 6112-6216.
14. S. Kilina, D. Kilin and S. Tretiak, *Chem. Rev.*, 2015, **115**, 5929-5978.
15. T. A. Pham, Y. Ping and G. Galli, *Nat. Mater.*, 2017, **16**, 401-408.
16. D. R. Yarkony, *Rev. Mod. Phys.*, 1996, **68**, 985-1013.

17. D. R. Yarkony, *Chem. Rev.*, 2012, **112**, 481-498.
18. F. Bernardi, M. Olivucci and M. A. Robb, *Chem. Soc. Rev.*, 1996, **25**, 321-328.
19. B. G. Levine and T. J. Martinez, *Ann. Rev. Phys. Chem.*, 2007, **58**, 613-634.
20. S. Matsika and P. Krause, in *Annual Review of Physical Chemistry, Vol 62*, eds. S. R. Leone, P. S. Cremer, J. T. Groves and M. A. Johnson, Annual Reviews, Palo Alto, 2011, vol. 62, pp. 621-643.
21. W. Domcke and D. R. Yarkony, *Ann. Rev. Phys. Chem.*, 2012, **63**, 325-352.
22. M. S. Schuurman and A. Stolow, *Ann. Rev. Phys. Chem.*, 2018, **69**, 427-450.
23. K. Y. Cheng, R. Anthony, U. R. Kortshagen and R. J. Holmes, *Nano Lett.*, 2011, **11**, 1952-1956.
24. Y. Shu and B. G. Levine, *J. Phys. Chem. C*, 2014, **118**, 7669-7677.
25. Y. Shu, B. S. Fales and B. G. Levine, *Nano Lett.*, 2015, **15**, 6247-6253.
26. W. T. Peng, B. S. Fales, Y. N. Shu and B. G. Levine, *Chem. Sci.*, 2018, **9**, 681-687.
27. Y. N. Shu, B. S. Fales, W. T. Peng and B. G. Levine, *J. Phys. Chem. Lett.*, 2017, **8**, 4091-4099.
28. Y. Shu, U. R. Kortshagen, B. G. Levine and R. J. Anthony, *J. Phys. Chem. C*, 2015, **119**, 26683-26691.
29. W. Kohn and L. J. Sham, *Phys. Rev.*, 1965, **140**, 1133-1138.
30. E. K. U. Gross and W. Kohn, *Phys. Rev. Lett.*, 1985, **55**, 2850-2852.
31. M. E. Casida, C. Jamorski, K. C. Casida and D. R. Salahub, *J. Chem. Phys.*, 1998, **108**, 4439-4449.
32. B. G. Levine, C. Ko, J. Quenneville and T. J. Martinez, *Mol. Phys.*, 2006, **104**, 1039-1051.
33. Y. H. Shao, M. Head-Gordon and A. I. Krylov, *J. Chem. Phys.*, 2003, **118**, 4807-4818.
34. N. Minezawa and M. S. Gordon, *J. Phys. Chem. A*, 2009, **113**, 12749-12753.
35. S. Gozem, F. Melaccio, A. Valentini, M. Filatov, M. Huix-Rotllant, N. Ferre, L. M. Frutos, C. Angeli, A. I. Krylov, A. A. Granovsky, R. Lindh and M. Olivucci, *J. Chem. Theory Comput.*, 2014, **10**, 3074-3084.
36. J. M. Herbert, X. Zhang, A. F. Morrison and J. Liu, *Acc. Chem. Res.*, 2016, **49**, 931-941.
37. Y. Yang, L. Shen, D. Zhang and W. T. Yang, *J. Phys. Chem. Lett.*, 2016, **7**, 2407-2411.
38. Y. N. Shu, K. A. Parker and D. G. Truhlar, *J. Phys. Chem. Lett.*, 2017, **8**, 2107-2112.
39. Y. N. Shu, K. A. Parker and D. G. Truhlar, *J. Phys. Chem. A*, 2017, **121**, 9728-9735.
40. Q. Wu, C. L. Cheng and T. Van Voorhis, *J. Chem. Phys.*, 2007, **127**, 164119.
41. G. L. Manni, R. K. Carlson, S. J. Luo, D. X. Ma, J. Olsen, D. G. Truhlar and L. Gagliardi, *J. Chem. Theory Comput.*, 2014, **10**, 3669-3680.
42. S. Pijeau and E. G. Hohenstein, *J. Chem. Theory Comput.*, 2017, **13**, 1130-1146.
43. J. W. Snyder, R. M. Parrish and T. J. Martinez, *J. Phys. Chem. Lett.*, 2017, **8**, 2432-2437.
44. B. O. Roos and P. R. Taylor, *Chem. Phys.*, 1980, **48**, 157-173.
45. B. G. Levine, M. P. Esch, B. S. Fales, D. T. Hardwick, W.-T. Peng and Y. Shu, *Ann. Rev. Phys. Chem.*, 2019, **70**, 21-43.
46. B. S. Fales and B. G. Levine, *J. Chem. Theory Comput.*, 2015, **11**, 4708-4716.
47. E. G. Hohenstein, N. Luehr, I. S. Ufimtsev and T. J. Martinez, *J. Chem. Phys.*, 2015, **142**, 224103.
48. I. S. Ufimtsev and T. J. Martinez, *J. Chem. Theory Comput.*, 2009, **5**, 1004-1015.
49. I. S. Ufimtsev and T. J. Martinez, *J. Chem. Theory Comput.*, 2009, **5**, 2619-2628.
50. Y. Shu, E. G. Hohenstein and B. G. Levine, *J. Chem. Phys.*, 2015, **142**.
51. C. W. Bauschlicher and S. R. Langhoff, *J. Chem. Phys.*, 1988, **89**, 4246-4354.

52. A. S. Demeras, M. B. Lepetit and J. P. Malrieu, *Chem. Phys. Lett.*, 1990, **172**, 163-168.
53. Y. N. Shu and B. G. Levine, *J. Chem. Phys.*, 2013, **139**, 074102.
54. J. M. Bofill and P. Pulay, *J. Chem. Phys.*, 1989, **90**, 3637-3646.
55. D. M. Potts, C. M. Taylor, R. K. Chaudhuri and K. F. Freed, *J. Chem. Phys.*, 2001, **114**, 2592-2600.
56. M. L. Abrams and C. D. Sherrill, *Chem. Phys. Lett.*, 2004, **395**, 227-232.
57. G. Granucci, M. Persico and A. Toniolo, *J. Chem. Phys.*, 2001, **114**, 10608-10615.
58. P. Slavicek and T. J. Martinez, *J. Chem. Phys.*, 2010, **132**, 234102.
59. Z. Lu and S. Matsika, *J. Chem. Theory Comput.*, 2012, **8**, 509-517.
60. B. S. Fales, E. G. Hohenstein and B. G. Levine, *J. Chem. Theory Comput.*, 2017, **13**, 4162-4172.
61. E. G. Hohenstein, *J. Chem. Phys.*, 2016, **145**, 174110.
62. B. S. Fales, Y. Shu, B. G. Levine and E. G. Hohenstein, *J. Chem. Phys.*, 2017, **147**, 094104.
63. N. Koga and K. Morokuma, *Chem. Phys. Lett.*, 1985, **119**, 371-374.
64. M. J. Bearpark, M. A. Robb and H. B. Schlegel, *Chem. Phys. Lett.*, 1994, **223**, 269-274.
65. S. Zilberg and Y. Haas, *Chem. Eur. J*, 1999, **5**, 1755-1765.
66. D. R. Yarkony, *J. Phys. Chem. A*, 2004, **108**, 3200-3205.
67. C. Ciminelli, G. Granucci and M. Persico, *Chem. Eur. J*, 2004, **10**, 2327-2341.
68. B. G. Levine, J. D. Coe and T. J. Martinez, *J. Phys. Chem. B*, 2008, **112**, 405-413.
69. K. Andersson, P. A. Malmqvist and B. O. Roos, *J. Chem. Phys.*, 1992, **96**, 1218-1226.
70. J. Finley, P. A. Malmqvist, B. O. Roos and L. Serrano-Andres, *Chem. Phys. Lett.*, 1998, **288**, 299-306.
71. S. M. Prokes, W. E. Carlos and V. M. Bermudez, *Appl. Phys. Lett.*, 1992, **61**, 1447-1449.
72. B. K. Meyer, V. Petrovakoch, T. Muschik, H. Linke, P. Omling and V. Lehmann, *Appl. Phys. Lett.*, 1993, **63**, 1930-1932.
73. M. Lannoo, C. Delerue and G. Allan, *J. Lumines.*, 1993, **57**, 243-247.
74. N. P. Brawand, M. Voros and G. Galli, *Nanoscale*, 2015, **7**, 3737-3744.
75. J. M. Buriak, *Chem. Comm.*, 1999, **1999**, 1051-1060.
76. A. B. Sieval, R. Linke, H. Zuilhof and E. J. R. Sudholter, *Adv. Mater.*, 2000, **12**, 1457-1460.
77. W. R. Wadt and P. J. Hay, *J. Chem. Phys.*, 1985, **82**, 284-298.
78. J. Michl and V. Bonacic-Koutecky, *Electronic Aspects of Organic Photochemistry*, Wiley, New York, 1990.
79. M. Garavelli, F. Bernardi, P. Celani, M. A. Robb and M. Olivucci, *J. Photochem. Photobiol. A-Chem.*, 1998, **114**, 109-116.
80. B. G. Levine and T. J. Martinez, *J. Phys. Chem. A*, 2009, **113**, 12815-12824.
81. L. A. Heimbrook, B. E. Kohler and I. J. Levy, *J. Chem. Phys.*, 1984, **81**, 1592-1597.
82. Y. Shu and B. G. Levine, *J. Chem. Phys.*, 2013, **139**, 081102.
83. Y. Shu and B. G. Levine, *J. Phys. Chem. C*, 2015, **119**, 1737-1747.
84. Y. N. Shu and B. G. Levine, *J. Phys. Chem. C*, 2016, **120**, 23246-23253.
85. M. P. Esch, Y. Shu and B. G. Levine, *J. Phys. Chem. A*, 2019, Accepted, 10.1021/acs.jpca.1029b00952.
86. M. Olivucci, I. N. Ragazos, F. Bernardi and M. A. Robb, *J. Am. Chem. Soc.*, 1993, **115**, 3710-3721.

87. D. C. Hannah, J. H. Yang, P. Podsiadlo, M. K. Y. Chan, A. Demortiere, D. J. Gosztola, V. B. Prakapenka, G. C. Schatz, U. Kortshagen and R. D. Schaller, *Nano Lett.*, 2012, **12**, 4200-4205.
88. G. J. Atchity, S. S. Xantheas and K. Ruedenberg, *J. Chem. Phys.*, 1991, **95**, 1862-1876.
89. D. R. Yarkony, *J. Chem. Phys.*, 2001, **114**, 2601-2613.
90. R. A. Marcus, *J. Chem. Phys.*, 1956, **24**, 966-978.
91. P. F. Barbara, T. J. Meyer and M. A. Ratner, *J. Phys. Chem.*, 1996, **100**, 13148-13168.
92. M. V. Wolkin, J. Jorne, P. M. Fauchet, G. Allan and C. Delerue, *Phys. Rev. Lett.*, 1999, **82**, 197-200.

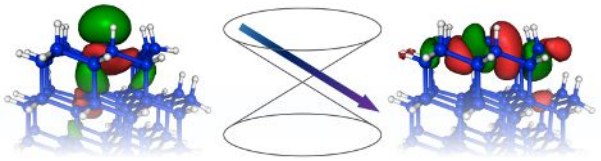

We review recent efforts to model nonradiative recombination in semiconductor nanoparticles through conical intersections, focusing on the reasons for and consequences of the locality of such intersections.